Magnetic Resonance Imaging with a Variable Field Superconducting Magnet that can be rotated for Vertical or Horizontal Operation

Sarah Vashaee[1], Ming Li[1], Bryce MacMillan[1], Razieh Enjilela[1], Derrick P. Green[2], F. Marica[1], Bruce J. Balcom[1]

[1] UNB MRI Research Centre, Department of Physics, University of New Brunswick, E3B 5A3, Canada

[2] Green Imaging Technologies, Inc., 520 Brookside Drive, Suite B Fredericton, NB, E3A 8V2, Canada

This paper was prepared for presentation at the International Symposium of the Society of Core Analysts held in Vienna, Austria, 28 August-1 September 2017

ABSTRACT

Magnetic Resonance (MR) is widely employed in the petroleum industry for down-hole logging and for laboratory core analysis. Sensitivity of the magnetic resonance experiment to fluid type and fluid environment makes it uniquely well suited to these applications. The same advantages should accrue to Magnetic Resonance Imaging (MRI) measurements of core flooding experiments. The ability of MRI to directly measure fluid saturation and fluid environment in three dimensions, as a function of time, has to this point, not been fully realized for core flood applications.

Bulk ^{1}H relaxation time measurements are near universally undertaken at low magnetic field to reduce magnetic susceptibility mismatch effects. These fields, typically 0.05 Tesla (2 MHz for ^{1}H), are too low for MRI studies. Higher magnetic fields (3 Tesla and above) are commonly employed for biomedical MRI studies with superconducting magnets. Susceptibility mismatch effects at these field strengths can be severe for many core plug samples and these higher field are generally inappropriate for rock core studies. What is the best field for petroleum core plug MRI studies? It will be sample dependent as one seeks to balance greater sensitivity at high field with susceptibility effects which decrease the transverse signal lifetimes (T_2 and T_2*) as field increases.

New generation superconducting magnets, actively cooled rather than passively cooled, are permanently connected to the magnet power supply and thus have the possibility of variable field operation. We have recently installed a variable field superconducting magnet MRI instrument which permits operation in the field range 0.01 Tesla to 3 Tesla. This magnet permits one to maximize the sample magnetization for high sensitivity core flooding MRI measurements, while controlling the effect of susceptibility mismatch on the signal lifetime. Because of the elimination of liquid cryogens the new magnet is a fraction of the size and weight of conventional superconducting magnets. The magnet can easily be rotated, from horizontal to vertical, by one person.

Variable field operation permits MRI measurement of other nuclei of interest and importance in core flooding studies. The gyromagnetic ratio of sodium ^{23}Na and fluorine ^{19}F are each less than that of hydrogen ^{1}H but one may increase the static field strength to compensate for the decrease in gyromagnetic ratio such that the RF probe employed to excite and detect the MRI signal has an unchanged frequency. This provides the experimentalist an entirely new way to undertake multi-nuclear MRI studies of core plug systems.

INTRODUCTION

Magnetic Resonance (MR) and Magnetic Resonance Imaging (MRI) are commonly employed for rock core and petroleum studies. MRI resolves structure in rock core plugs under study, as does X-ray CT. The MRI measurement is however a direct measurement of the ^{1}H containing fluids in the core plug, unlike X-ray measurements where absorption is principally due to the matrix [1]. In addition, the MRI measurement has the potential to investigate different nuclei, for example sodium, but more importantly is sensitive to the local dynamics and environment of the fluid. A very wide variety of MR measurements may be spatially resolved with MRI, including measurements of fluid self-diffusion and velocity. MR/MRI measurements may be interpreted to yield a wealth of petrophysical information including fluid viscosity, fluid type, fluid saturation, rock wettability, permeability, capillary pressure and the pore size distribution [2-11]

The fact that MR/MRI can measure so many different petrophysical parameters, with so many different protocols, is a practical weakness when compared to the simpler X-ray CT measurement. Which MR/MRI measurement should be executed, and how, is a common question. This highlights the importance of expert advice and experience in petrophysical MR/MRI studies.

There is considerable interest in monitoring oil displacement processes with Magnetic Resonance Imaging (MRI) methodologies to understand and improve enhanced oil recovery. The ability of MRI to directly measure fluid saturation and fluid environment in three dimensions as a function of time has not been fully realized for core flood applications because of long measurement times at low magnetic fields which can hamper monitoring the displacement [12, 13]. 1D and 2D MRI measurements are instead often undertaken to monitor the oil displacement since they are faster. Although these images may characterize well the overall oil distribution in a homogeneous core sample, the image may be misleading in a heterogeneous core plug, or for a process which is heterogeneous. Fast Spin Echo (FSE) imaging methods have been applied to investigate the 3D fluid content in core-plugs [2, 13].

^{1}H relaxation time measurements are generally performed at low field to reduce magnetic susceptibility mismatch effects. These fields, typically 0.05 Tesla (2 MHz for ^{1}H) with permanent magnets, are too low for MRI studies. The shift to low-field is accompanied by an essential reduction in signal-to-noise ratio. Biomedical MRI is usually conducted at

higher magnetic field strengths with superconducting magnets. MR spectroscopy studies of molecular structure are usually undertaken with high field superconducting magnets.

Higher magnetic fields for MRI provides better SNR and therefore allows high sensitivity and higher resolution imaging, in principle. However, the magnetic susceptibility mismatch decreases the T_2^* in rock cores which hinders both resolution and contrast with conventional high speed MRI methods. The B_0 field distortion in the pore space due to susceptibility mismatch creates so called 'internal' magnetic field gradients. The strength of the internal magnetic field gradients scales with B_0 and the susceptibility mismatch ($\Delta\chi$). It is important to know the best static magnetic field for petroleum core plug MRI studies to balance greater sensitivity at high field with susceptibility effects which decrease the transverse signal lifetimes (T_2 and T_2*) as field increases. A decrease in the T_2^* lifetime manifests as a less of signal intensity in pure phase encode SPRITE MRI images [14], as shown below. A decrease in T_2^* and T_2 due to susceptibility contrast results in a loss of signal intensity, loss of resolution and may lead to geometric distortion in frequency encode measurements, such as the fast spin echo method employed below.

New generation cryogen free superconducting magnets, actively cooled rather than passively cooled, are permanently connected to the magnet power supply and consequently have the option of variable field operation. We have recently installed a variable field superconducting magnet MRI Instrument which permits operation in the field range 0.01 Tesla to 3 Tesla. This magnet permits one to maximize the sample magnetization for high sensitivity core flooding MRI measurements, while controlling the effect of susceptibility mismatch on the signal lifetime. The cryogen free variable field magnet is a field changing magnet, it is not a field cycling magnet. Fast field cycling is increasingly employed for T_1 dispersion measurements in petroleum systems [15, 16].

A cryogen free magnet with active cooling permits one to enjoy the benefits of a superconducting magnet, which includes field homogeneity and temporal field stability without employing liquid helium. Liquid helium is required as a cryogen for conventional superconducting magnets. Helium cost and stability of supply are of increasing concern in many parts of the word. Permanent magnet based MR/MRI instruments are well-known to suffer from poor innate field homogeneity and temporal field instability due to ambient temperature change.

Due to the elimination of liquid cryogens for cooling, the new magnet is a fraction of the size and weight of conventional, liquid-based, superconducting magnets. The new magnet is small enough and light enough to permit rotation. The ability to rotate the magnet is advantageous for experiments in which the sample orientation matters, for example when gravity and buoyancy are important [17]. Examples include gas injection in petroleum systems, including two phase gas-liquid flow.

We show in this paper results from the variable field magnet in which nuclei (^{1}H and ^{19}F) were employed for core flood imaging. The ^{19}F resonance is ideally suited for MR imaging

since it has a high gyromagnetic ratio, spin 1/2, and 100% natural isotopic abundance [18]. One pulse ^{1}H Free Induction Decay (FID) results are shown during magnet rotation. We also show MR measurement of ^{23}Na in a brine saturated rock core plug. The same RF probe was employed for ^{1}H and ^{23}Na experiments but the magnetic field was changed to maintain the same resonance frequency.

EXPERIMENTAL

MR/MRI measurements were performed on a variable field magnet, maximum field 3T (MR Solutions, Guildford, Surrey, UK) with a 17 cm bore. The RF probe was a birdcage (Barthel HF-Technik, Aachen, Germany). The magnet is 325 kg, 66 cm in diameter and 80 cm in length. It was initially configured for operation at 0.79 T, 1.5 T and 3T. The 3D gradient coil was driven by gradient amplifiers (Performance Controls, Inc., PA, US), providing maximum gradient strengths of 66.4 G/cm, 64.9 G/cm and 87.8 G/cm in the *x, y* and *z* directions. The magnet is permanently connected to a magnet power supply (Cryomagnetics, Inc., TN, US).

3D Conical-SPRITE MRI measurements were undertaken on three different rock core plugs (Bentheimer and Berea (Kocurek Industries, Caldwell, TX), and Wallace (Wallace Quarries Ltd., NS, Canada)), length 5 cm and diameter 3.8 cm, at both 1.5 T and 3 T. All three core plugs were fully saturated with 2% brine. SPRITE imaging parameters were: signal averages = 2, field of view = 100×100×100 mm^3, 64^3 k-space points were acquired each with a phase encoding time of 100 μs. The T_1 recovery delays were 2s, 800 ms and 400 ms for Bentheimer, Berea and Wallace core plugs, respectively. The 90° pulse duration was 63 μs at 1.5 T and 38 μs at 3 T. The RF flip angle was 10° for SPRITE measurements.

For flooding measurements Fluorolube oil MO-10 (Gabriel Performance Products, OH, United States) was utilized as the oil phase. The viscosity of the fluorinated oil was 50 mPa s at 25 °C. H_2O brine, 1 wt% NaCl, was employed for core plug saturation. A Bentheimer core plug (Kocurek Industries, TX, USA) was employed with length 5.1 cm, diameter 3.8 cm, pore volume 13 cm^3 and a porosity of 23%. The pore volume was calculated gravimetrically. An ISCO pump (Teledyne ISCO, Lincoln, NE, US) was employed for fluid injection. A homemade low pressure core holder was employed for flooding experiments.

The Bentheimer core plug was dried at 100 °C to a constant weight and then saturated with 1 wt% NaCl H_2O brine. The pore volume of the core plug was calculated gravimetrically. FID, 3D conical SPRITE [19] and 3D Fast Spin Echo (FSE) MRI measurements were undertaken at 1.5 T for ^{1}H.

To establish the initial oil saturation, fluorinated oil was injected into the core plug with a syringe until no water production was observed at the outlet end. The initial oil volume inside the sample was 10.2 ml which provides an initial oil saturation of 0.79. FID and 3D FSE measurements were performed at both 1.5 T for ^{1}H and 1.6 T for ^{19}F. 3D SPRITE MRI was undertaken at 1.5 T for ^{1}H. Change of nucleus was achieved by changing the

static magnetic field strength with the resonance frequency constant at 63.5 MHz (no change in RF probe).

H_2O brine, 1 wt% NaCl, was employed to displace the fluorinated oil. FID and 3D FSE measurements were undertaken at 1.6 T for ^{19}F to monitor the oil displacement. The sample and the magnet were horizontal. The flooding measurement ceased when the FID signal intensity was constant. After displacement of the oil with H_2O brine, approximately 4.3 ml oil remained inside the sample. Water flooding was undertaken at ambient temperature. The water flooding flow rate was 0.045 ml/min.

2D slice-selective FSE measurements were undertaken to monitor the progression of flooding. The FSE measurement required 16 signal averages with a total imaging time of 12 minutes. The acquisition is sufficiently fast to permit observation of the flooding front displacement. 34 slices (Figure 4) were acquired in the *x* direction to give a 3D data set. The slice thickness was 1.2 mm. 16 k-space frequency encode lines (spin echoes) were acquired per excitation. The echo time was 8 ms. The center of k-space was acquired with the first echo. The field of view was 7 cm in the frequency and phase encode directions. The repetition time between each excitation was 2s. The 2D images were 128×128 pixels.

Preclinical scan software (MR Solutions, Guildford, Surrey, UK) was employed to execute the FSE MRI images. A home built MATLAB program (MathWorks, Natick, MA, USA, written in MATLAB) was employed to visualize 3D FSE images. GIT system software (Green Imaging Technologies, Inc., NB, Canada) was employed to execute FID, CPMG and double-half-k SPRITE [19] measurements.

RESULTS AND DISCUSSION

Variation of B_0 to control sensitivity and susceptibility mismatch effects

The variable field superconducting magnet MRI Instrument permits operation in the field range 0.01 Tesla to 3 Tesla. This permits one to maximize the sample magnetization for high sensitivity core flooding MRI measurements, while controlling the effect of magnetic susceptibility mismatch on T_2^* and T_2. Chen and Balcom have shown [14] that the internal magnetic field distortion is proportional to the external magnetic field strength (B_0) and the susceptibility difference ($\Delta\chi$). The single exponential T_2^* behavior observed arises from an effective Lorentzian distribution of the internal field, induced by the large susceptibility contrast and an intrinsic disordered pore structure. The linewith ($1/(\pi T_2^*)$) measured at different magnetic field strengths (B_0) for a Chatsworth Formation sandstone, water saturated Berea and a carbonate are shown in Figure 1. The slope differs for each sample due to a different susceptibility mismatch ($\Delta\chi$). The new data point corresponds to a new brine saturated Berea plug measured with the new magnet set to 3T.

Figure 2 shows, 2D planes extracted from the 3D SPRITE images for Bentheimer, Berea and Wallace core plugs at both 1.5 T and 3 T. The image intensity for Berea and Wallace core plug images is decreased at higher field. Short T_2^* lifetimes of water in the Berea and Wallace core plugs at 3 T diminish the sensitivity of the SPRITE measurement [14].

However, for the Bentheimer core plug with substantially longer T_2^* the image intensity increases when the B_0 field increases from 1.5 T to 3 T. The image intensity is a balance between sample magnetization which increases with B_0 field strength, sample porosity which varies between the three samples, and T_2^* which varies with the sample and decreases with field strength.

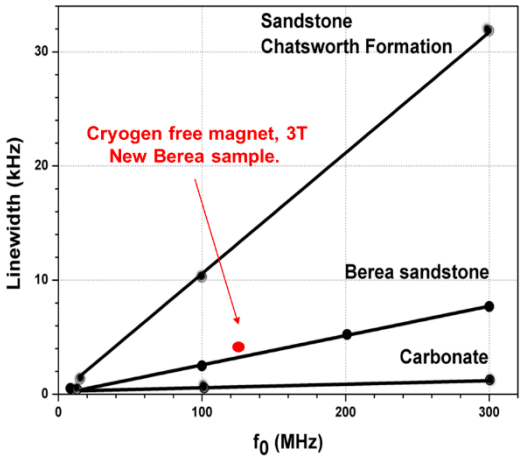

Figure 1. The linewidth ($1/(\pi T_2^*)$) measured at different magnetic field strengths (B_0) for a Chatsworth Formation sandstone, water saturated Berea sandstone and a Carbonate. The measurements at frequencies other than 125 MHz were performed on other MRI instruments in the UNB MRI center. There is a linear relationship between the linewidth and the product of the $\Delta\chi$ and Larmor frequency (f_0). The best fit line for a Berea sandstone is given by $\Delta\nu = 0.26\ \Delta\chi\ f_0$.

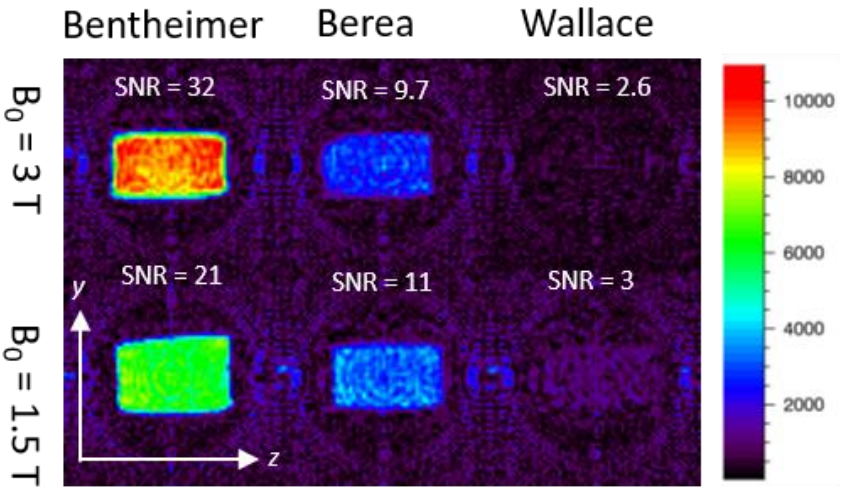

Figure 2. 2D slice images of Bentheimer, Berea and Wallace core plugs from 3D SPRITE images at 3 T and 1.5 T. For each sample a slice from the centre of the 3D core plug image is displayed. There is a probe background signal apparent in all images. Measurement time was 8.5 minutes, 7 minutes and 6 minutes for Bentheimer, Berea and Wallace core plugs, respectively. In each case, 2 signal averages were acquired; the difference in measurement time is due to the T_1 recovery delay. The signal-to-noise ratio (SNR) varies due porosity differences between the core plugs, but also due to sample magnetization change with field, and with the field dependent T_2* lifetime variation of water in the pore space.

Magnet rotation

The cryogen free magnet is small enough and light enough to permit rotation. Measurement at different orientations is very advantageous for petroleum flooding measurements in which gravity and buoyancy may be important. The one pulse ^{1}H FIDs from a doped water phantom were measured during magnet rotation at 3 T. The FID results with different magnet orientations are shown in Figure 3. When the magnet rotates from horizontal to vertical, as shown in Figures 2a-2c, the FID goes off resonance but the field homogeneity in the sample space (T_2^*) is unchanged. When the magnet is horizontal, the earth's field (0.5 gauss) is at right angles to B_0 (30,000 gauss) and thus there is no effect on the resonance frequency. When the earth's field and the static field B_0 are co-linear, in the vertical orientation, the addition of the two fields changes the Larmor frequency. The predicted change is an increase in frequency of 2 kHz. An increase of 1.95 kHz was observed.

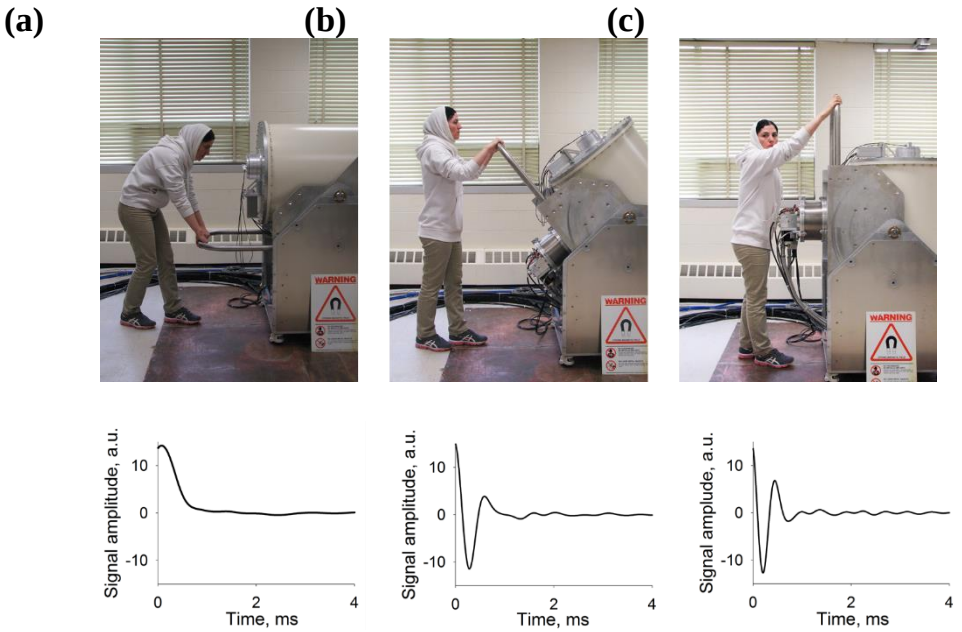

Figure 3. FIDs from a doped water sample acquired during magnet rotation. The Gifford-McMahon (GM) cryocooler permits vertical or horizontal operation (indeed any orientation) unlike a pulse tube cryocooler. The magnet may be easily rotated by one person.

Multi-field, multi-frequency operation

Switch from ^{1}H at 1.5 T to ^{19}F at 1.6 T with fixed 63.5 MHz frequency RF probe

Figure 4 shows the oil saturation distribution in 2D FSE slices for a Bentheimer core plug during water flooding. The average initial oil saturation was 0.79 in the core plug.

Water flooding displaced oil to an average residual oil saturation of 0.33. A non-piston like displacement was apparent. High intensity oil signal was observed at the interface of the

PEEK distributor and the core plug. The oil signal intensity is proportional to oil saturation. An inhomogeneous initial oil saturation was observed.

Higher water saturation is observed at one end of the core plug (Figure 4). This may be due to a capillary end effect for the short sample [20]. The ^{1}H images of the fully brine saturated Bentheimer, before flooding and after flooding are shown in Figure 4. Change of nucleus to ^{1}H was achieved by changing the static magnetic field strength. The resonance frequency was constant at 63.5 MHz. The same RF probe was used for both ^{1}H and ^{19}F imaging measurements.

If the sample T_2 is longer than tens of ms, and T^*_2 is not less than 1 ms, frequency encode spin echo MRI measurements, such as the 2D slice-selective FSE, are suggested for rapid fluid saturation imaging in core flooding studies. The measurement time of 12 minutes ensured high quality images in our studies. The measurement time may be reduced to 5 minutes with a decrease in SNR. If the T_2 is less than tens of ms, or the T^*_2 is less than 1 ms, then a Centric Scan SPRITE method is recommended for fluid saturation imaging, although the imaging time will increase.

Switch from ^{1}H at 0.79 T to ^{23}Na at 3 T with fixed 33.7 MHz RF frequency
Variable field operation also permits MR measurement of ^{23}Na with the same RF probe employed for ^{1}H measurements. ^{1}H and ^{23}Na FID signals, 1D double-half-k profiles and T_2 distributions for a fully 2% brine saturated Bentheimer sample are shown in Figure 5.

The T_2^* was approximately 1.6 ms for both ^{23}Na and ^{1}H (Figures 4a and 4b). As expected, for the same measurement time (2.5 minutes), the ^{1}H and ^{23}Na measurements signal to noise ratios differ by a factor of 100. The ^{1}H signal has higher SNR.

The T_2 distribution for ^{1}H in the Bentheimer core plug has two peaks, T_{2peak} = 400 ms and 28 ms. The ^{23}Na T_2 distribution was unimodal, T_{2peak} = 44 ms. CPMG experiment parameters for ^{1}H T_2 measurement were: echo time = 2.6 ms, number of echoes = 1541, number of averages = 32 and recycle delay = 6 s. The CPMG parameters for ^{23}Na T_2 measurement were: echo time = 2.6 ms, number of echoes = 193, number of averages 128 and recycle delay = 2 s. The measurement time for CPMG measurement was approximately 5.5 minutes. For the same measurement time for ^{1}H and ^{23}Na measurements the SNR for the ^{1}H signal is 160 time larger than that for ^{23}Na signal. The 90° pulse length and magnetic field gradient strengths employed for ^{23}Na measurements were approximately four times greater than that for ^{1}H measurement ($\gamma_{23Na}/\gamma_{1H}$ = 3.8).

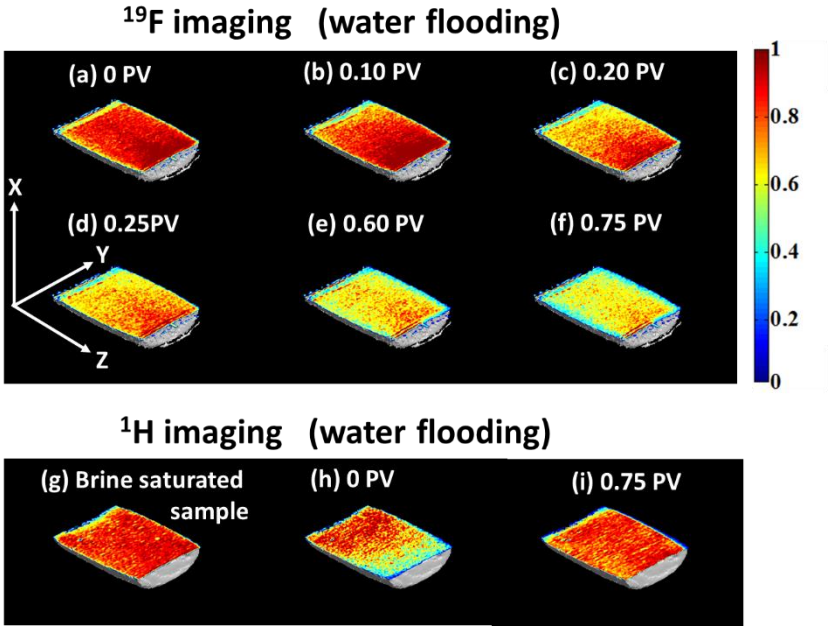

Figure 4. (a-f) The oil saturation distribution ^{19}F, 2D FSE image slices, superimposed on a cut 3D image background for a Bentheimer core plug during water flooding. The observed signal is solely from oil. The flooding is from $-z$ to z. The average initial oil saturation in (a) was 0.79. Water flooding displaced the oil (b-f) to a residual oil saturation of 0.33 in (f). The oil saturation is directly proportional to the signal intensity. The water saturation distribution from ^{1}H 2D FSE image slices, is shown in (g-i) superimposed on a cut 3D image background for the same Bentheimer core plug before and after the same flooding experiment. Image (g) shows the sample fully saturated with brine; the signal is solely from water, (h) shows the sample saturated with brine and oil (before flooding) while (i) shows the sample after flooding has ceased. Images (b) and (h) correspond to the commencement of flooding. The water and oil saturation distribution is inhomogeneous in these two images. The measurements were done at 1.5 T for ^{1}H, 1.6 T for ^{19}F. Change of nucleus was achieved by changing B_0. The resonance frequency was constant at 63.5 MHz.

^{23}Na MR/MRI can be employed as a complementary approach to conventional ^{1}H MR/MRI for shale fluid typing, taking advantage of the fact that sodium ions are only present in the aqueous phase. ^{23}Na can also be used for investigating brine salinity effects in porous media including conventional rocks, clays, and shale, and may be employed to differentiate hydrocarbon and aqueous phases [3, 21-25].

CONCLUSION

A cryogen free superconducting magnet system is introduced for petroleum MR/MRI studies. The small size and light weight of the magnet (by comparison to conventional superconducting magnets) permits one to rotate the magnet. The cryogen free superconducting magnet permits B_0 field change because the magnet power supply is permanently connected. The ability to change the static magnetic field makes it possible to control susceptibility effects in rock core plugs and to resonate different nuclei (^{19}F, ^{23}Na) by employing a constant frequency RF probe.

The new magnet was employed for core flooding MRI measurements at 1.5 T for ^{1}H and at 1.6 T for ^{19}F. It also permits one to perform ^{23}Na measurements for a brine saturated Bentheimer sandstone at 3 T with a resonance frequency of 33.7 MHz. Variable field operation is very advantageous for samples with susceptibility driven inhomogeneous broadening since one can readily control the experimental line width $1/(\pi T_2^*)$ [14].

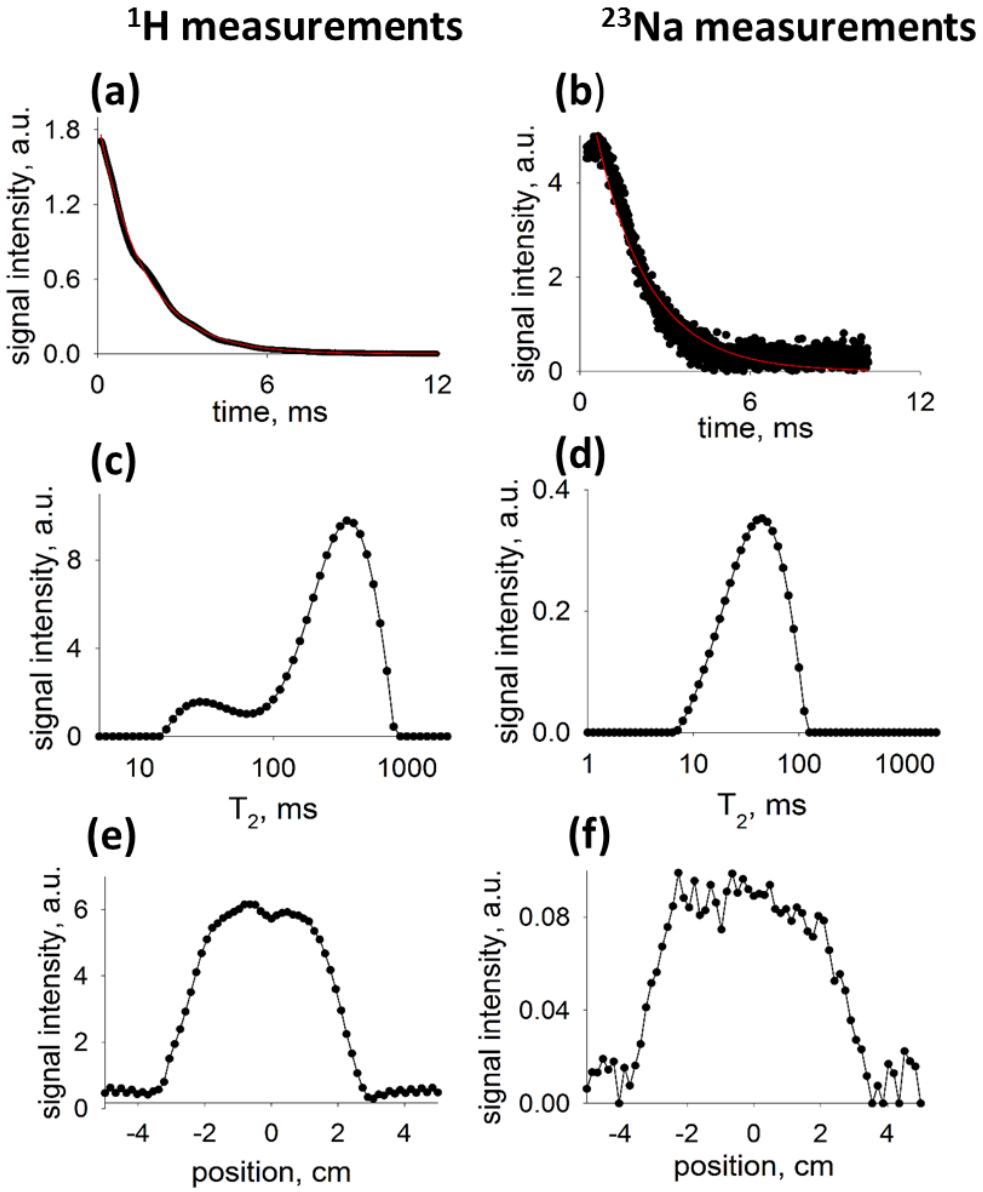

Figure 5. FID signal of brine saturated Bentheimer core plug (2% NaCl) for (a) ^{1}H and (b) ^{23}Na, the red lines are the fitted plots. (c) ^{1}H T_2 distribution, (d) ^{23}Na T_2 distribution. The ^{1}H T_2 distribution has two components reflecting the pore size distribution. The ^{23}Na T_2 distribution is unimodal. 1D double half-k SPRITE profile for (e) ^{1}H (proton density profile) and (f) ^{23}Na in Bentheimer core plug (salinity profile). FOV is 10 cm with phase encoding time of 400 us.

ACKNOWLEDGEMENTS

BJB thanks NSERC of Canada for a Discovery grant and the Canada Chairs program for a Research Chair in MRI of Materials. The authors also thank Green Imaging Technologies, ConocoPhillips, Saudi Aramco, the Atlantic Innovation Fund and the New Brunswick Innovation Fund for financial support. S. Vashaee thanks Jean-Marc S. Belliveau for helping with data visualization.

REFERENCES

1. C.T. P Chang and A.T. Watson, NMR Imaging of Flow Velocity in Porous Media, AIChE Journal, 45 (1999) 437-444.
2. J. Mitchell, T.C. Chandrasekera, D.J. Holland, F.L. Gladden, E.J. Fordham. Magnetic Resonance Imaging in Laboratory Petrophysical Core Analysis, Phys. Rep. 526 (2013) 165-225.
3. J. Mitchell. Magnetic Resonance Core Analysis at 0.3 T. SCA2014-010, International Symposium of the Society of Core Analysts, Avignon, France, Sept. 8-11, 2014
4. Y. Zhao, Y. Song, Y. Liu, H. Liang, B. Dou. Visualization and Measurement of CO_2 Flooding in Porous Media using MRI, Ind. Eng. Chem. Res. 50 (2011) 4707-4715.
5. D. Green, D. Veselinovic, B.J. Balcom, F. Marica. Applications of a New Technique to Acquire Spatially Resolved NMR Petrophysical Data. SCA2012-32, International Symposium of the Society of Core Analysts, Aberdeen, Scotland, UK, Aug. 27-30, 2012.
6. R. Freedman. Advances in NMR Logging, J. Pet. Technol. 58 (2006) 60-66.
7. A. Brautaset, G. Ersland, A. Graue, J. Stevens, J. Howard. Using MRI to Study in-situ Oil Recovery during CO_2 Injection in Carbonates. SCA2008-41, International Symposium of the Society of Core Analysts, Abu Dhabi, UAE, Oct. 29-Nov. 2, 2008.
8. D. Green, J. Dick, M. McAloon, P.F. de J. Cano-Barrita, J. Burger, B. Balcom. Oil/Water Imbibition and Drainage Capillary Pressure Determined by MRI on a Wide Sampling of Rocks. SCA2008-01, International Symposium of the Society of Core Analysts, Abu Dhabi, UAE, Oct. 29-Nov. 2, 2008.
9. G.R. Coates, L. Xiao, M.G. Prammer. NMR Logging Principles and Applications; Halliburton Energy Services: Houston, USA, 1999.
10. M. Li, D. Xiao, M. Shakerian, A. Afrough, F. Goora, F. Marica, L. Romero-Zerón, B. Balcom, Magnetic Resonance Imaging of Core Flooding in a Metal Core Holder. SCA2016-064, International Symposium of the Society of Core Analysts, Colorado, USA, Aug. 21-Aug. 26, 2016.
11. C.E. Muir, O.V. Petrov, K.V. Romanenko, B.J. Balcom, Measuring Miscible Fluid Displacement in Porous Media with Magnetic Resonance Imaging Water Resour. Res. 50 (2014), 1859–1868.
12. M. Li, D. Xiao, L. Romero-Zerón, F. Marica, B. MacMillan, B.J. Balcom, Mapping Three-Dimensional Oil Distribution with π-EPI MRI Measurements at Low Magnetic Field, J. Magn. Reson. 269 (2016) 13-23.
13. M. Li, D. Xiao, L. Romero-Zerón, B.J. Balcom. Monitoring Oil Displacement Processes with *k*-t Accelerated Spin Echo SPI, Magn. Reson. Chem. 54 (2016) 197-204.

14. Q Chen, A.E. Marble, B.G. Colpitts, B.J. Balcom, The Internal Magnetic Field Distribution, and Single Exponential Magnetic Resonance Free Induction Decay, in Rocks, J. Magn. Reson. 175 (2005) 300-308.
15. E. Anoardo', G. Galli, G. Ferrante, Fast-Field-Cycling NMR: Applications and Instrumentation, Appl. Magn. Reson. 20 (2001) 365-404.
16. J.P. Korb, G. Freiman, B. Nicot, P. Ligneul, Dynamical Surface Affinity of Diphasic Liquids as a Probe of Wettability of Multimodal porous media, Phys. Rev. B. 061601 (2009) 1-12.
17. K. Alba, S. M. Taghavi, I. A. Frigaard, Miscible Heavy-light Displacement Flows in an Inclined Two-dimensional Channel: A Numerical Approach, Phys. Fluids. 26 (2014) 1-22.
18. G.N. Holland, P.A. Bottomley, W.S. Hinshaw, ^{19}F Magnetic Resonance Imaging, J. Mag. Reson. 136 (1977).
19. M. Halse, D.J. Goodyear, B. MacMillan, P. Szomolanyi, D. Matheson, B.J. Balcom, Centric Scan SPRITE Magnetic Resonance Imaging, J. Magn. Reson. 165 (2003) 219-229.
20. K. Romanenko, B.J. Balcom, An Assessment of Non-wetting Phase Relative Permeability in Water-wet Sandstones Based on Quantitative MRI of Capillary End Effects, J. Petrol. Sci. Eng. 110 (2013) 225-231.
21. D. Yang, R. Kausik, ^{23}Na and ^{1}H NMR Relaxometry of Shale at High Magnetic Field, Energy Fuels, 30 (2016) 4509-4519.
22. K. E. Washburn, G. Madelin. Imaging of Multiphase Fluid Saturation within a Porous Material via Sodium NMR. J. Magn. Reson. 202 (2010) 122−126.
23. P. Tutunjian, H. Vinegar, J. Ferris, Nuclear Magnetic Resonance Imaging of Sodium-23 in Cores. Log Analyst. 34 (1993), 34 (03) 11-18.
24. H.T. Hu, L.Z. Xiao, X.L. Wu, Corrections for Downhole NMR Logging. Pet. Sci. 9 (2012), 46−52.
25. J. Mitchell, E.J. Fordham, Contributed Review: Nuclear Magnetic Resonance Core Analysis at 0.3 T, Rev. Sci. Instrum. 85 (2014) 1-17.